Hindawi
Advances in Civil Engineering
Volume 2024, Article ID 2818930, 12 pages
https://doi.org/10.1155/2024/2818930

Research Article

Mechanical Performance Investigation of a Flat-Roof and Four-Slope Folded Plate Structure

Yan Yang[1], **Meng Zhan**[1] **and Yanfei Huang**[2]

[1]*College of Civil Engineering and Architecture Huanghuai University, Zhumadian 463000, China*
[2]*Qianjiang Urban Planning and Design Institute, Qianjiang 433100, China*

Correspondence should be addressed to Yan Yang; 20111222@huanghuai.edu.cn

Received 11 October 2023; Revised 1 March 2024; Accepted 14 March 2024; Published 10 April 2024

Academic Editor: Afaq Ahmad

The flat-roof and four-slope folded plate structure is a space thin-walled structure composed of four trapezoidal plates and a rectangular plate parallel to the bottom surface, which is widely used in various engineering applications. In order to clarify the force transmission path and stress distribution law under the action of this structural load, the folded plate structures were made by utilizing the plexiglass with the thicknesses of 3 and 4 mm, respectively, and had the simple support on opposite sides and fixed support on another opposite side. Then, the static load tests and ANSYS finite element analysis were implemented, and the results were compared. It shows that the test results are basically consistent with the finite element calculation results, the maximum stress values of the folded plate structure along the X and Y directions appear in the same position, and the maximum stress value of a 3 mm thick folded plate structure is greater than that of 4 mm. The junction position of the roof and the slope plate is the dangerous section, and the special treatment should be made for this section to prevent the damage of folded plate structure in the practical engineering. Moreover, some reasonable measures also should be taken to meet the design requirements of the plate–plate junction position.

1. Introduction

The folded plate structure is a space thin-walled structure composed of several flat plates. It has the inherent characteristics of the plate and thin shell structures. This structure has clear force, short force transmission route, lightweight, high rigidity, and it is materials saving. In addition to better seismic performance, it is easy for construction and time-saving that is found in on-site fabrication of flat plates [1–4]. With the improvement of experimental research and better understanding of engineering practice, the application of folded plate structures becomes wider, such as roof factory buildings, residential buildings, auditoriums, and movie theaters.

The forms that are commonly used of folded plate structure are groove shape, V shape, combined folded plate, etc. At present, the focus is on the mechanical properties of this type of structure and related theoretical and experimental research. For example, Lai et al. [5] studied the simply supported V-shaped folded plate roof. Ding et al. [6] studied based on the finite element analysis software for the structure under two different support forms with arch angle four-point support and surrounding multipoint support. The results show that under the two support conditions, the fundamental frequency of the structure is most affected by the rise-span ratio, and the rise-span ratio of the structure is recommended to be 1/5. Guo et al. [7] studied the mechanical characteristics and design points of the composite beam roof with prestressed concrete V-shaped folded plate. Miao et al. [8] studied the dynamic performance of the complex double-layer folded plate reticulated shell and analyzed the modal, stability, and seismic performance of the structure. Zhu et al. [9] studied static characteristics of concrete prismatic folded-plate reticulated shells with dense ribs on oblique grids. Yu and Liu [10] conducted research on the characteristics and key technologies of a new type of folded grid shell structure. Zhang et al. [11] completed temperature strain measurement and analysis of large-volume concrete structures in large-span folded arch tunnels. Zhang [12] analyzed the dynamic performance of the polyhedral space folded-plate structure model by using Midas/gen and SAP2000 and studied the structure in multiple seismic performance under earthquake action. Gaafar [13] first considered the relative displacement of the folded plate joint in their method, which provided a reference for solving the

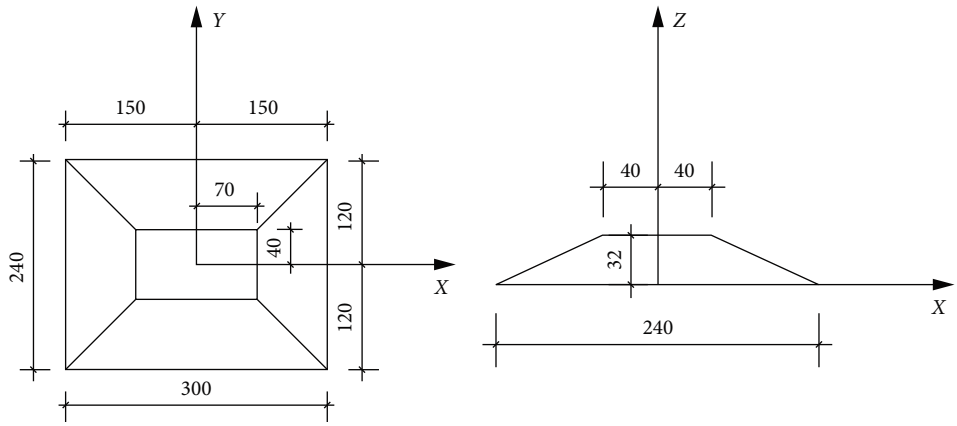

Figure 1: Schematic diagrams of flat-roof and four-slope folded plate structure: (a) plane view and (b) sectional view.

problems related to the folded plate more accurately. The work of Goldberg and Leve [14] was adopted by Guha-Niyogi et al. [15]. It is considered to be the first time that the exact solution of the static problem of the folded plate is given. Bandyopadhyay and Laad [16] reviewed and compared the approximate and exact analysis methods of the folded plate. Milašinović and Bursać [17] presented numerical analysis of typical folded-plate structures by the finite strip method (FSM) taking into account geometrical and material nonlinearity. Yousif et al. [18] presented an optimum design algorithm for reinforced concrete folded plate structures.

Flat-roofed folded plates are composed of four trapezoidal plates and a rectangular plate parallel to the bottom surface. As a new type of spatial structure, the folded plate structure has the advantages of lightweight structure, economical material use, simple construction, and so on, and it is still in the initial stage of study. Now it mainly focuses on the mechanical properties analysis under the boundary condition of four sides simply supported and temperature load. Lai [19] established the surface equation of the flat-roof and four-slope folded plate roof with the help of the local oblique coordinate system and generalized functions (sign function and step function). The elastic thin shell theory and the variational method are applied, and the expressions of the deflection and internal force of the four-sided simply supported flat-roof and four-slope folded plate roof are derived. This research group has done a lot of work on flat-roof and four-slope folded plate structures, mainly studying the variation laws of stress–strain curve, load–displacement curve, and other mechanical properties of such structures under the condition of simple support on four sides and the action of conventional loads and temperature loads [20, 21]. At the same time, the mechanical properties and seismic response numerical analysis were conducted on flat-roof and four-slope folded plate structures with simple support on opposite sides and fixed support on another opposite side, and the results showed that the damage was most severe at the interface between the plates, which was the weak part of the structure [22, 23].

However, there are few reports on the force transfer path and stress distribution of the folded plate structure with a flat roof and four slopes with simple support on opposite sides and fixed support on another opposite side. Based on the previous study on the flat-roof and four-slope folded plate structure with 3 mm thickness in the X direction, the paper further investigated the mechanical properties of the flat-roof and four-slope folded plate structure with different thicknesses in the X and Y directions and obtained the stress, strain, and displacement at key parts of the structure, providing guidance for the design and application of folded plate structure in practical engineering.

2. Mechanics Performance Test

2.1. Test Model Design. The model is made by precisely cutting of plexiglass plates and processed by hands, and the plates are glued together with glue to precisely control the angle between the plates of the folded plate structure and the contact area between the plates. In this experiment, plexiglass plates with the thicknesses of 3 and 4 mm were selected as the structural material and base material of the folded plate structure. During the model-making process, the two long sides were fixed, and the two short sides were in a simply supported state. Model size: bottom side length $a = 150$ mm, $b = 120$ mm; top plate side length $a0 = 70$ mm, $b0 = 40$ mm; sagittal height $f = 32$ mm; and thickness $h = 3$ or 4 mm respectively, as shown in Figure 1.

The elastic modulus and Poisson's ratio of 3 and 4 mm thick plexiglass materials were measured by electrical measurement (Figure 2), and the results are as follows: (a) 4 mm thick plexiglass plate: $E = 3.649$ GPa, $\mu = 0.333$, and (b) 3 mm thick plexiglass plate: $E = 3.249$ GPa, $\mu = 0.331$.

2.2. Test Point Arrangement and Loading Process. During the test loading process, in order to prevent the concentrated force from directly acting on the glass surface from causing the damage, the loading force was transmitted to the four joints between the top plate and slope plate through the steel plate, as shown in Figure 3. MTS810 Material Test System equipment is used for loading, and DH3816 and DH3817 strain acquisition instruments are used for test data collection, on both sides of the three special Sections 1-1, 2-2, and

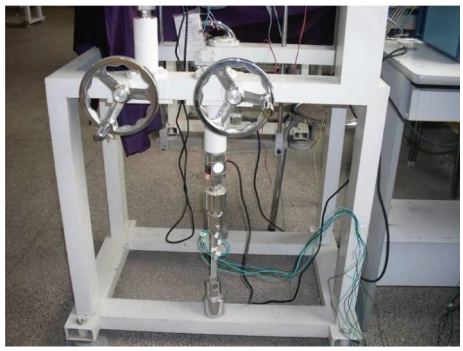

Figure 2: Experiment loading device.

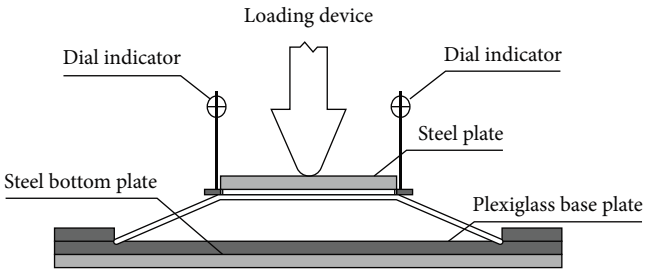

Figure 3: Schematic diagram of specimen loading.

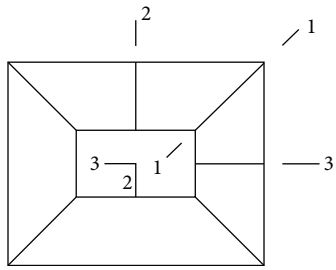

Figure 4: Schematic diagram of special cross-section position.

3-3 on the outer surface of the four slopes and the upper part of the top plate, strain gauges are placed at the position, as shown in Figure 4. The dial indicator contacts are installed on the small plexiglass rods drawn from the four corners of the top plate to monitor the vertical displacement of the top plate. The maximum range of the dial indicator is 10 mm.

Using the step-by-step loading method, the loading value of each stage is 10% (50 N) of the design load value, and the loading is completed in 12 stages. It takes 1 min from the beginning of loading to the completion of loading for each stage. From the end of loading to the next level of loading, the duration is 10 min, so that the internal force redistribution of the specimen can be completed, and the next level of loading is applied after the deformation under a certain level of loading is basically stable. The test data are read manually after it is stabilized. The test loading process is shown in Figure 5.

2.3. Test Results and Analysis. When the load exceeds 400 N, for the plexiglass model material, the stress at this time can already produce 2,000 macrostrains. To ensure sufficient accuracy of the measured values, only the load range of 300 N for the folded plate structure is used for experimental research.

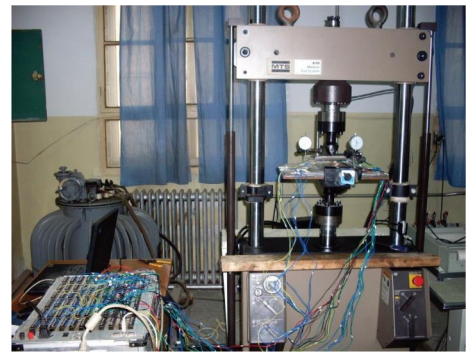

Figure 5: Model test loading process diagram.

Table 1 shows the displacement values of the top plate of the folded plate structure measured in the test. The displacement and strain of the structure basically tend to be linear during the step-by-step loading. Tables 2 and 3 present the strain at each section of the folded plate structure. The position of the maximum strain value along the X and Y directions for the two folded plate structures with different thicknesses is the same.

3. Finite Element Analysis

3.1. Model Establishment. With the development of computer technology, numerical methods gradually play an important role in structural analysis, and finite element method [24–27] has been introduced to solve engineering structural problems. The SHELL63 unit of ANSYS is selected to simulate the plexiglass plate, and the specific parameters of the model are consistent with the taken experimental parameters. When dividing the unit, the SHELL63 unit is divided into hexahedral units, in which case the calculation is more stable and easier to converge, and the specific modeling is shown in Figure 6.

3.2. Calculation Results and Analysis. Through ANSYS software modeling and analysis, the calculation of the displacement, stress, and strain values of Sections 1-1, 2-2, and 3-3 for the folded plate structure with different thicknesses under the step-by-step loading from 50 to 300 N is carried out, as shown in Tables 4–9.

When the load is 300 N for 3 mm model, the maximum displacement on Section 1-1 occurs at $x = 52.5$ mm, $y = 30$ mm, $w = -5.968 \times 10^{-2}$ mm. The maximum stress in the X direction is at $x = 52.5$ mm, $y = 30$ mm, $\sigma_X = 2.517$ MPa, the maximum stress in the Y direction is at $x = 52.5$ mm, $y = 30$ mm, $\sigma_Y = 2.309$ MPa.

When the load is 300 N for 3 mm model, the maximum displacement on Section 2-2 occurs at $x = 0$ mm, $y = 0$ mm, $w = -3.125 \times 10^{-2}$ mm. The maximum stress in the X direction is at $x = 0$ mm, $y = 0$ mm, $\sigma_X = -0.718$ MPa, and the maximum stress in the Y direction is at $x = 0$ mm, $y = 0$ mm, $\sigma_Y = 0.174$ MPa.

Table 1: Test displacement values of the top plate of the folded plate structure.

Model (mm)	Measuring point	Load value (N)					
		50	100	150	200	250	300
3	Left side	−0.0099	−0.0199	−0.0298	−0.0398	−0.0498	−0.0597
	Right side	−0.0099	−0.0202	−0.0304	−0.0404	−0.0504	−0.0602
	Mean value	−0.0099	−0.0201	−0.0301	−0.0401	−0.0501	−0.0600
4	Left side	−0.0069	−0.0129	−0.0188	−0.0248	−0.0308	−0.0356
	Right side	−0.0069	−0.0135	−0.0194	−0.0256	−0.0316	−0.0363
	Mean value	−0.0069	−0.0132	−0.0191	−0.0252	−0.0314	−0.0360

Table 2: Test strain values of each section of 3 mm thick folded plate structure.

Cross-section	Position (mm)		Load value (N)					
			50	100	150	200	250	300
1-1	X-axis	0	−30	−61	−91	−122	−153	−183
		70	2	5	7	9	13	14
		110	−1	−2	−4	−5	−6	−7
	Y-axis	0	16	32	48	65	81	97
		70	−7	−15	−22	−29	−36	−43
		110	−2	−5	−7	−10	−13	−16
2-2	X-axis	0	−30	−61	−91	−122	−143	−182
		40	−10	−20	−29	−39	−49	−59
		80	−8	−16	−24	−32	−40	−48
	Y-axis	0	16	32	48	65	82	97
		40	−5	−9	−14	−18	−22	−28
		80	−8	−15	−23	−31	−39	−46
3-3	X-axis	0	−30	−61	−91	−122	−152	−182
		70	−11	−22	−33	−44	−55	−66
		110	−18	−36	−55	−73	−91	−109
	Y-axis	0	16	33	48	65	82	97
		70	−27	−53	−80	−106	−132	−158
		110	3	5	7	10	13	16

Table 3: Test strain values of each section of 4 mm thick folded plate structure.

Cross-section	Position (mm)		Load value (N)					
			50	100	150	200	250	300
1-1	X-axis	0	−21	−43	−64	−85	−107	−126
		70	6	12	18	24	30	36
		110	−1	−2	−3	−4	−6	−8
	Y-axis	0	11	21	32	42	53	64
		70	0.5	0.9	1	2	2.3	2.7
		110	−2	−4	−6	−9	−11	−13
2-2	X-axis	0	−21	−43	−64	−85	−107	−129
		40	−9	−17	−26	−34	−43	−52
		80	−6	−11	−17	−23	−28	−33
	Y-axis	0	11	21	32	42	53	64
		40	−5	−9	−13	−18	−22	−23
		80	−5	−11	−16	−21	−27	−33
3-3	X-axis	0	−21	−43	−64	−85	−107	−129
		70	−8	−16	−24	−32	−40	−49
		110	−12	−25	−37	−50	−62	−76
	Y-axis	0	11	21	32	42	53	64
		70	−19	−38	−56	−75	−94	−113
		110	2	5	7	9	12	15

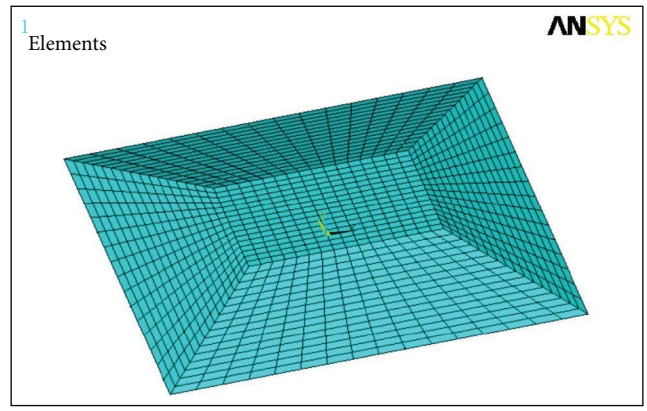

Figure 6: Finite element model of the folded plate structure.

Table 4: Mechanical properties of Section 1-1 of 3 mm model.

Position (mm)	Displacement ($\times 10^{-2}$ mm)	σ_X (MPa)	σ_Y (MPa)	Strain ε_X ($\times 10^{-3}$)	Strain ε_Y ($\times 10^{-3}$)
0	−3.125	−0.718	0.174	−0.182	0.097
30	−5.968	2.517	2.309	0.412	0.347
60	−0.710	−0.111	−0.153	−0.013	−0.026
90	0.123	−0.067	−0.084	−0.008	−0.014
120	0.000	−0.006	−0.032	−0.001	−0.000

Table 5: Mechanical properties of Section 2-2 of 3 mm model.

Position (mm)	Displacement ($\times 10^{-2}$ mm)	σ_X (MPa)	σ_Y (MPa)	Strain ε_X ($\times 10^{-3}$)	Strain ε_Y ($\times 10^{-3}$)
0	−3.125	−0.718	0.174	−0.182	0.097
30	−1.537	−0.563	−0.083	−0.126	0.0244
60	0.119	−0.477	−0.265	−0.088	−0.022
90	0.183	−0.244	−0.334	−0.027	−0.055
120	0.000	−0.106	−0.273	−0.000	−0.053

Table 6: Mechanical properties of Section 3-3 of 3 mm model.

Position (mm)	Displacement ($\times 10^{-2}$ mm)	σ_X (MPa)	σ_Y (MPa)	Strain ε_X ($\times 10^{-3}$)	Strain ε_Y ($\times 10^{-3}$)
0	−3.125	−0.718	0.174	−0.182	0.097
17.5	−3.731	−0.586	0.012	−0.138	0.064
35	−4.959	−0.459	−0.274	0.013	−0.062
44.75	−5.248	−0.503	−0.581	0.095	−0.153
61.25	−4.105	−0.820	−1.037	0.061	−0.238
90	−1.613	−0.478	−0.527	−0.066	−0.081
120	−0.472	−0.523	−0.085	−0.110	0.027
150	0.000	−0.420	−0.159	−0.081	0.001

When the load is 300 N for 3 mm model, the maximum displacement on Section 3-3 occurs at $x = 44.75$ mm, $y = 0$ mm, and $w = -5.248 \times 10^{-2}$ mm. The maximum stress in the X direction is at $x = 61.25$ mm, $y = 0$ mm, and $\sigma_X = -0.820$ MPa, the maximum stress in the Y direction is at $x = 61.25$ mm, $y = 0$ mm, $\sigma_Y = -1.037$ MPa.

When the load is 300 N for 4 mm model, the maximum displacement on Section 1-1 occurs at $x = 52.5$ mm, $y = 30$ mm, $w = -3.571 \times 10^{-2}$ mm. The maximum stress in the X direction is at $x = 52.5$ mm, $y = 30$ mm, $\sigma_X = 1.769$ MPa, and the maximum stress in the Y direction is at $x = 52.5$ mm, $y = 30$ mm, $\sigma_Y = 1.612$ MPa.

Table 7: Mechanical properties of Section 1-1 of 4 mm model.

Position (mm)	Displacement ($\times 10^{-2}$ mm)	σ_X (MPa)	σ_Y (MPa)	Strain ε_X ($\times 10^{-3}$)	Strain ε_Y ($\times 10^{-3}$)
0	−1.925	−0.559	0.109	−0.128	0.064
30	−3.571	1.769	1.612	0.265	0.220
60	−0.536	−0.143	−0.176	−0.016	−0.026
90	0.075	−0.060	−0.075	−0.007	−0.011
120	−0.000	−0.044	−0.019	−0.006	−0.003

Table 8: Mechanical properties of Section 2-2 of 4 mm model.

Position (mm)	Displacement ($\times 10^{-2}$ mm)	σ_X (MPa)	σ_Y (MPa)	Strain ε_X ($\times 10^{-3}$)	Strain ε_Y ($\times 10^{-3}$)
0	−1.925	−0.559	0.109	−0.128	0.064
30	−1.052	−0.482	−0.102	−0.096	0.013
60	−0.152	−0.390	−0.213	−0.066	−0.016
90	−0.001	−0.190	−0.263	−0.019	−0.040
120	0.000	−0.087	−0.225	0.000	−0.040

Table 9: Mechanical properties of Section 3-3 of 4 mm model.

Position (mm)	Displacement ($\times 10^{-2}$ mm)	σ_X (MPa)	σ_Y (MPa)	Strain ε_X ($\times 10^{-3}$)	Strain ε_Y ($\times 10^{-3}$)
0	−1.925	−0.559	0.109	−0.128	0.064
17.5	−2.280	−0.430	0.027	−0.096	0.042
35	−3.009	−0.327	−0.193	0.004	−0.038
44.75	−3.213	−0.402	−0.395	0.057	−0.095
61.25	−2.737	−0.775	−0.732	0.036	−0.152
90	−1.407	−0.346	−0.355	−0.045	−0.048
120	−0.524	−0.390	−0.022	−0.076	0.021
150	0.000	−0.318	−0.121	−0.056	0.000

When the load is 300 N for 4 mm model, the maximum displacement on Section 2-2 occurs at $x = 0$ mm, $y = 0$ mm, $w = -1.925 \times 10^{-2}$ mm. The maximum stress in the X direction is at $x = 0$ mm, $y = 0$ mm, $\sigma_X = -0.559$ MPa, and the maximum stress in the Y direction is at $x = 0$ mm, $y = 0$ mm, $\sigma_Y = 0.109$ MPa.

When the load is 300 N for 4 mm model, the maximum displacement on Section 3-3 occurs at $x = 44.75$ mm, $y = 0$ mm, and $w = -3.213 \times 10^{-2}$ mm. The maximum stress in the X direction is at $x = 61.25$ mm, $y = 0$ mm, and $\sigma_X = -0.775$ MPa, and the maximum stress in the Y direction is at $x = 61.25$ mm, $y = 0$ mm, and $\sigma_Y = -0.732$ MPa.

The cloud diagrams of the stress calculation results of each section in the X, Y, and Z directions are shown in Figures 7–9.

Through the comparison of the above figures and tables, it is observed that the change laws of mechanical performances of the 3 and 4 mm folded plate structures tend to be consistent, and the maximum stress along the X and Y directions occurs at the same position. The maximum stress occurs at $x = 52.5$ mm and $y = 30$ mm for Section 1-1, at $x = 0$ mm and $y = 0$ mm for Section 2-2, and at $x = 61.25$ mm and $y = 0$ mm for Section 3-3. The maximum stress value of a 3 mm thick folded plate structure is greater than that of a 4 mm thick folded plate structure, and the 4 mm thick folded plate structure tends to be more linear and smoother overall. It is recommended to use a thicker folded plate structure in future engineering applications to ensure structural security.

4. Comparative Analysis of Test Results and ANSYS Calculation Results

4.1. Comparison of Roof Displacement. When the folded plate structures with two thicknesses are loaded from 50 to 300 N, the comparison results of the roof displacement test values and the ANSYS calculation values are shown in Figure 10. It can be seen that under the step-by-step loading for the folded plate structure, the linear relationship between the displacement of the roof and the load is good. As the loading force increases, the displacement of the roof also gradually increases.

4.2. Comparison between Special Section Stresses. When the folded plate structure with 3 mm thicknesses is loaded step by step at 300 N, the comparison results of the section stress

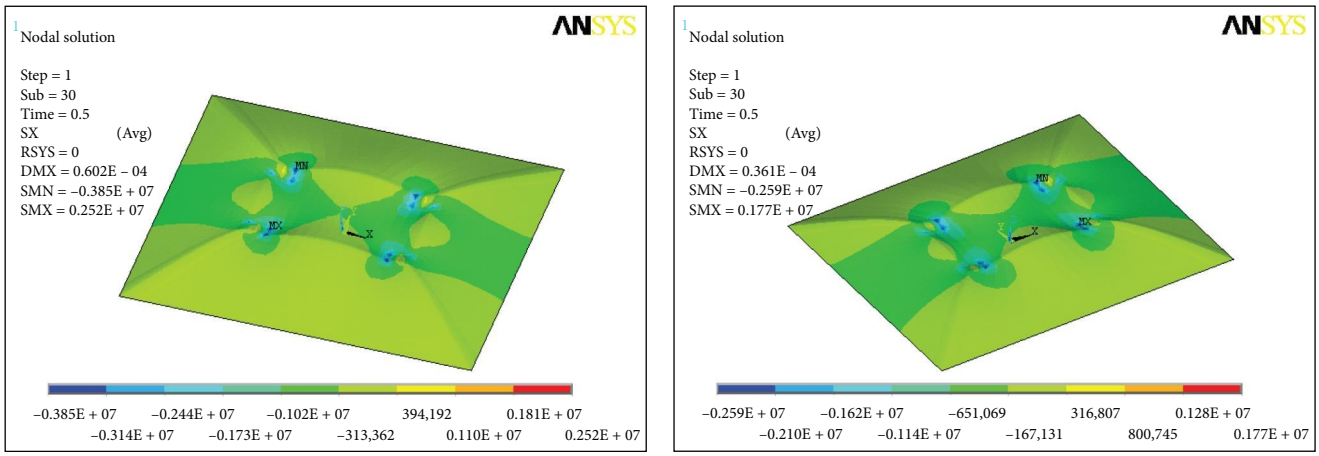

(a) (b)

Figure 7: Cloud diagrams of stress calculation results in X direction: (a) 3 mm model and (b) 4 mm model.

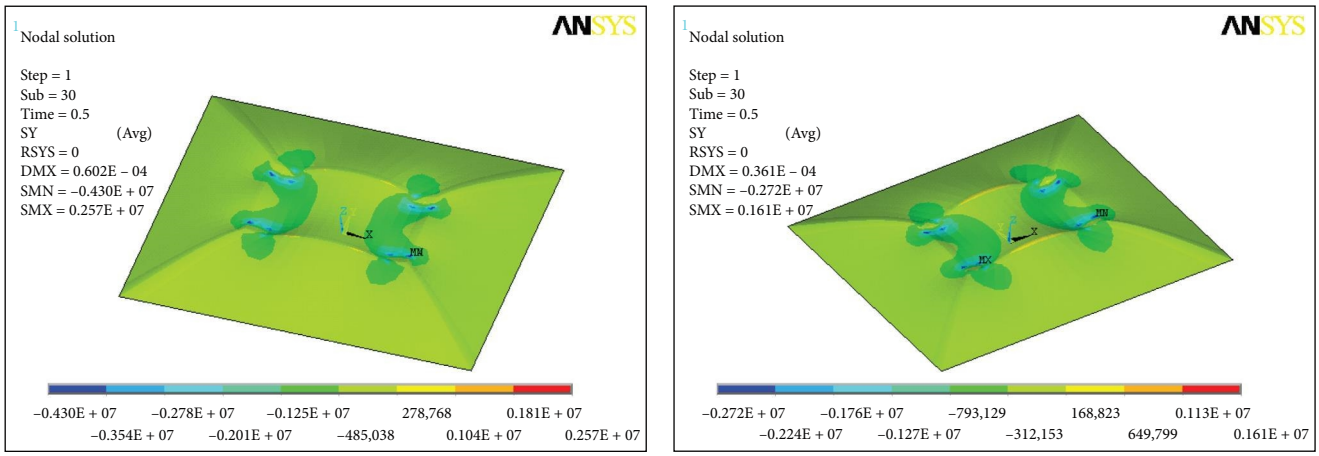

(a) (b)

Figure 8: Cloud diagrams of stress calculation results in Y direction: (a) 3 mm model and (b) 4 mm model.

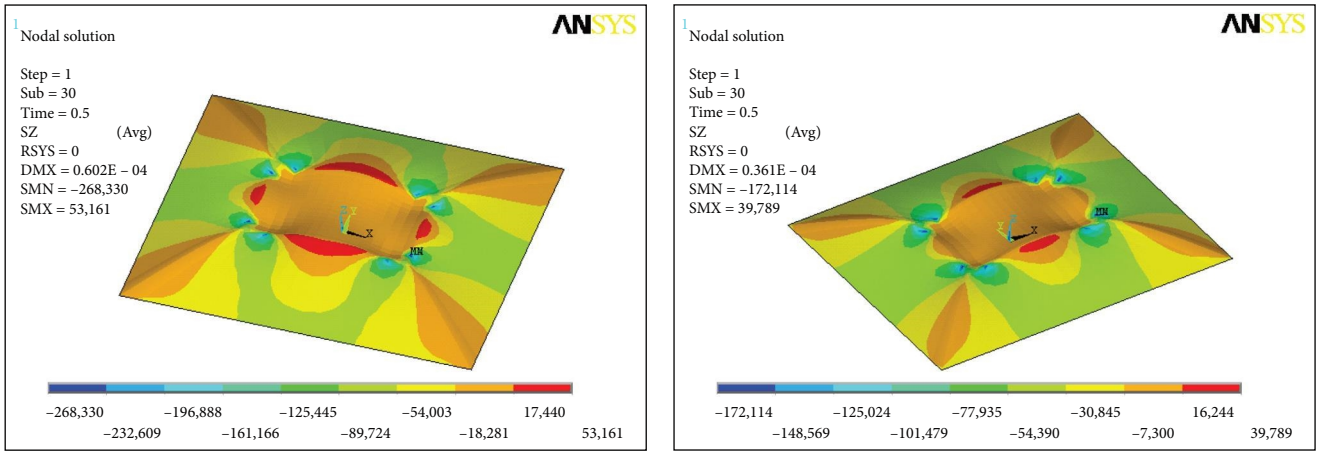

(a) (b)

Figure 9: Cloud diagrams of stress calculation results in Z direction: (a) 3 mm model and (b) 4 mm model.

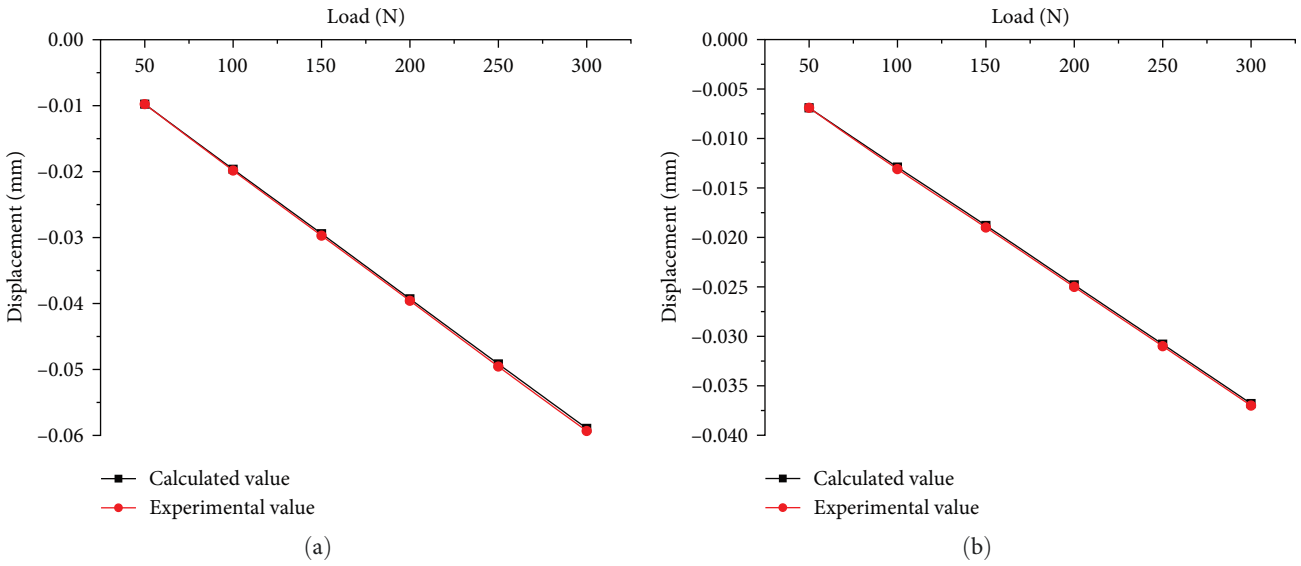

Figure 10: Comparison of test values and calculation values of roof displacement: (a) 3 mm model and (b) 4 mm model.

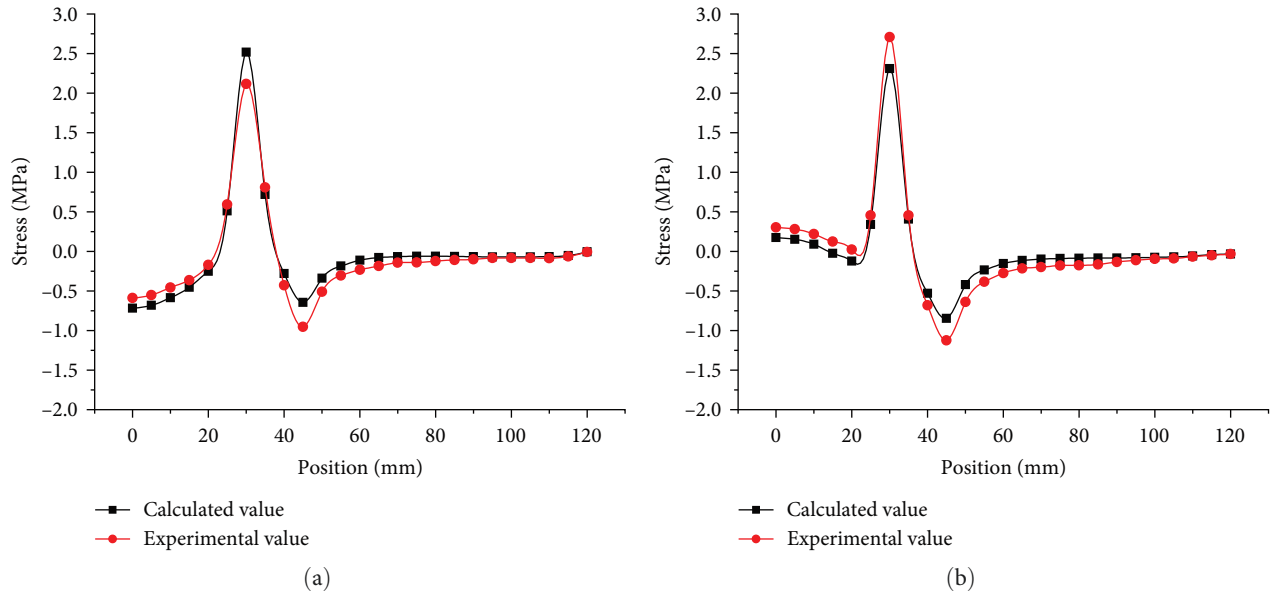

Figure 11: Relationship between stress and position on Section 1-1 of 3 mm model: (a) stress σ_X in X direction and (b) stress σ_Y in Y direction.

test value and the ANSYS finite element calculation value are shown in Figures 11–13. It can be seen that, in Section 1-1, the maximum stress along the X direction is 2.517 MPa and that is 2.309 MPa along the Y direction, the maximum stress in X and Y directions occurs at $x = 52.5$ mm and $y = 30$ mm. In Section 2-2, the maximum stress along the X direction is −0.718 MPa and that is 0.174 MPa along the Y direction, and the maximum stress in X and Y directions occurs at $x = 0$ mm and $y = 0$ mm. In Section 3-3, the maximum stress along the X direction is −0.072 MPa and that is −1.037 MPa along the Y direction, and the maximum stress in X and Y directions occurs at $x = 61.25$ mm and $y = 0$ mm.

When the folded plate structure with 4 mm thicknesses is loaded step by step at 300 N, the comparison results of the section stress test value and the ANSYS finite element calculation value are shown in Figures 14–16. It can be seen that, in Section 1-1, the maximum stress along the X direction is 1.769 MPa and that is 1.612 MPa along the Y direction, and the maximum stress in X and Y directions occurs at $x = 52.5$ mm and $y = 30$ mm. In Section 2-2, the maximum stress along the X direction is

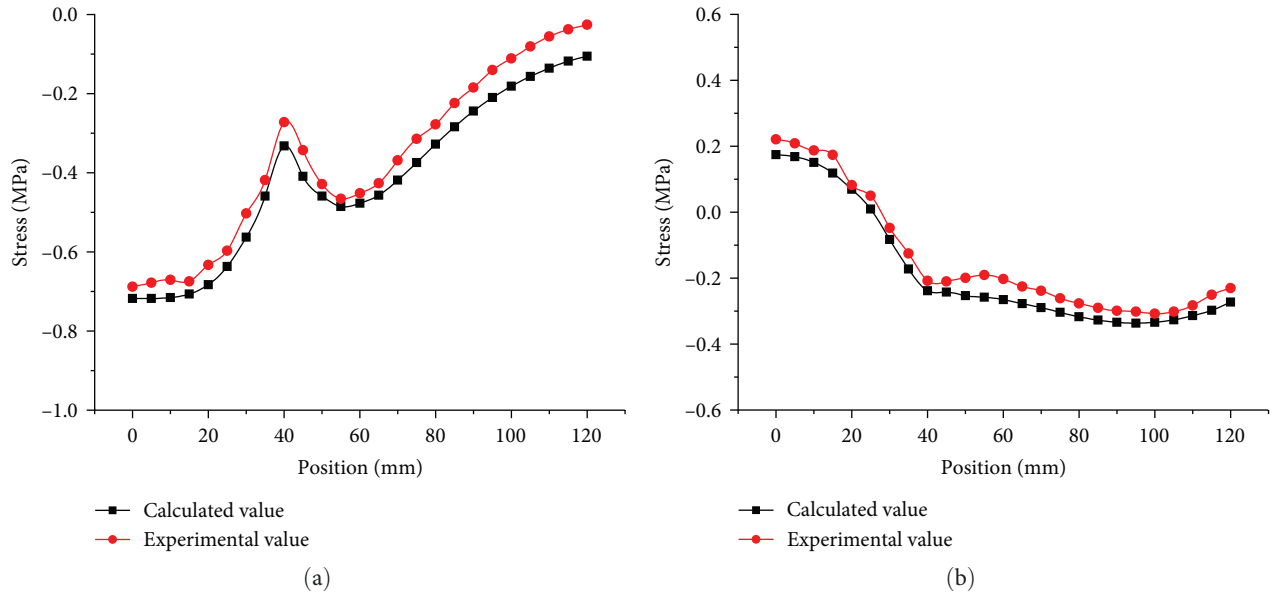

FIGURE 12: Relationship between stress and position on Section 2-2 of 3 mm model: (a) stress σ_X in X direction and (b) stress σ_Y in Y direction.

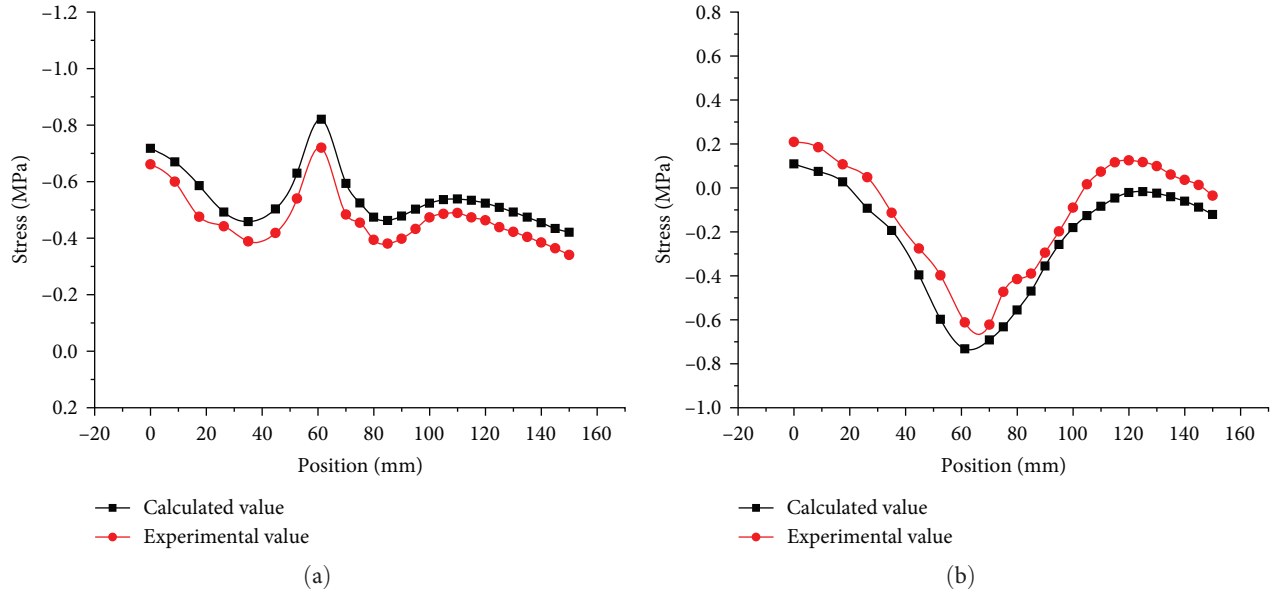

FIGURE 13: Relationship between stress and position on Section 3-3 of 3 mm model: (a) stress σ_X in X direction and (b) stress σ_Y in Y direction.

−0.559 MPa and that is 0.109 MPa along the Y direction, and the maximum stress in the X and Y directions occurs at $x = 0$ mm and $y = 0$ mm. In Section 3-3, the maximum stress along the X direction is −0.057 MPa and that is −0.732 MPa along the Y direction, and the maximum stress in X and Y directions occurs at $x = 61.25$ mm and $y = 0$ mm.

By comparing the stress–position relationship between Sections 1-1, 2-2, and 3-3 of flat-roof and four-slope folded plate structures with different thicknesses under the action of 300 N, it can be obviously observed that the maximum stress along the X and Y direction occurs at the same position whether the thickness of the structure is 3 or 4 mm. Generally speaking, the maximum stress is related to the factors such as the geometric shape and loading method of the specimens. At the joint position between the top plate and slope plates of the folded plate structure, the displacement and stress values are relatively large, forming the dangerous section of the structural damage. Meanwhile, the locally increased stress declines rapidly with the increase of the interval between the peak stress points. Special treatment

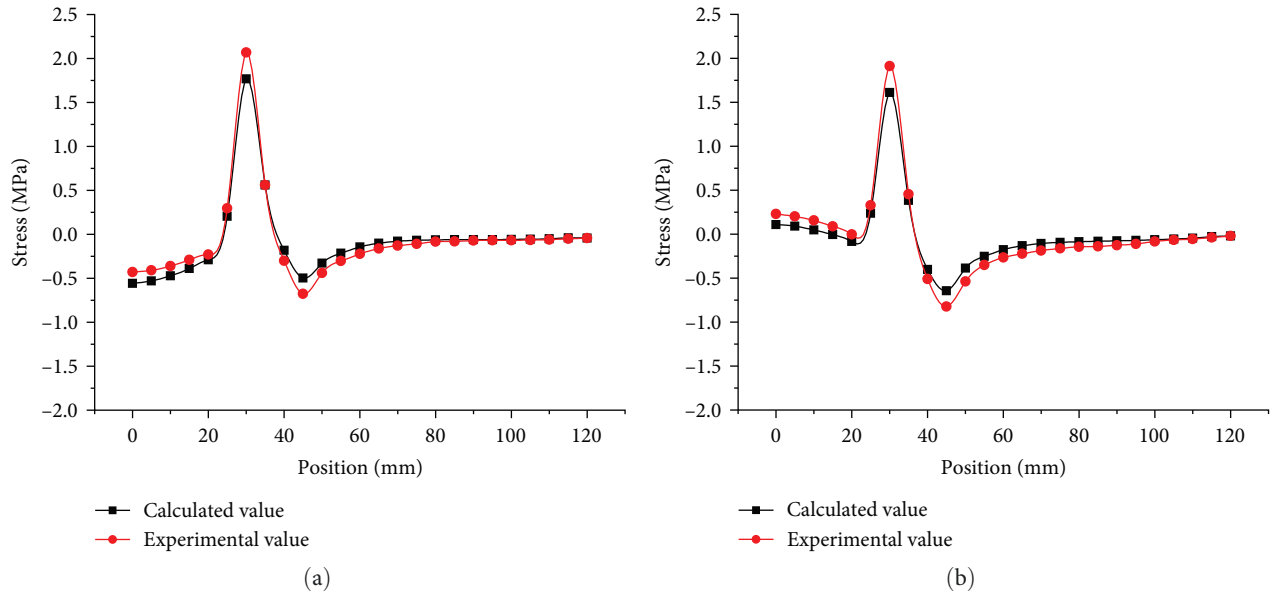

Figure 14: Relationship between stress and position on Section 1-1 of 4 mm model: (a) stress σ_X in X direction and (b) stress σ_Y in Y direction.

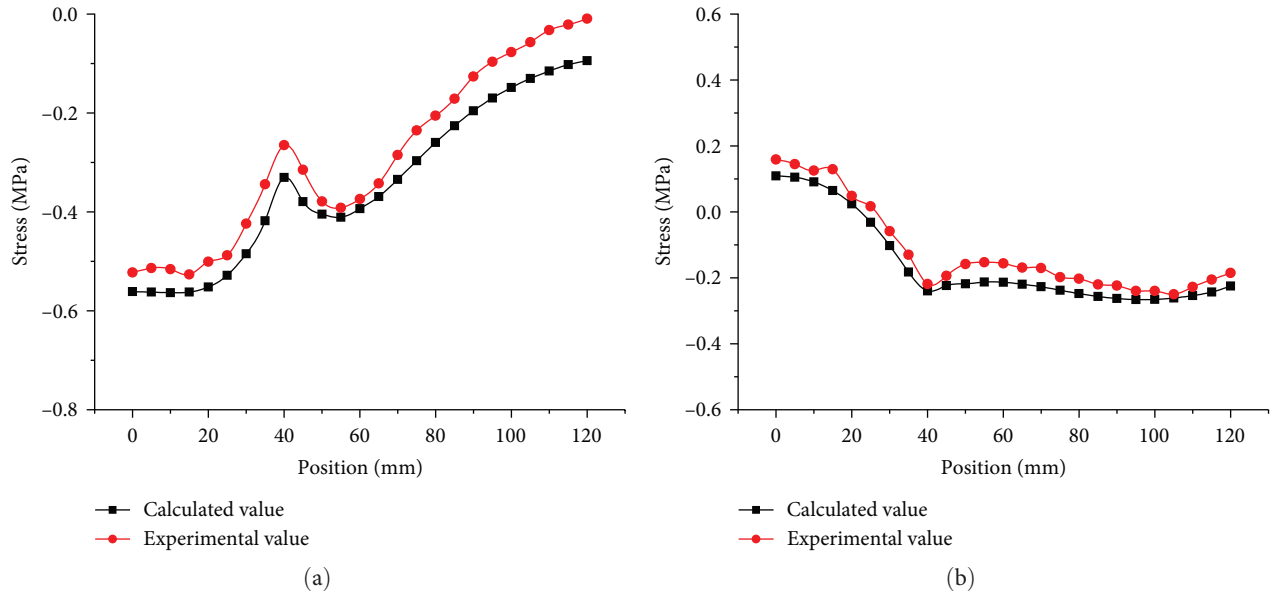

Figure 15: Relationship between stress and position on Section 2-2 of 4 mm model: (a) stress σ_X in X direction and (b) stress σ_Y in Y direction.

should be done for this section in practical engineering. For example, reinforced ribs can be added to enhance the strength of the section to prevent the damage.

5. Conclusions

By conducting the mechanical experiments of flat-roof and four-slope folded plate structures with thicknesses of 3 and 4 mm, the force transmission path and stress distribution law were analyzed; meanwhile, the ANSYS finite element analysis was carried out. The main conclusions of this work are as follows:

(1) The analysis of the experimental results shows that during the step-by-step loading process, the displacement and strain of the structure tend to be basically linear. The error between the experimental analysis results and the theoretical calculation results mainly lies in the loading position, constraint conditions, and adhesive materials, but these factors do not affect the applicability of linear theory. Throughout the entire destruction process, the structure exhibits good ductility overall. The comparison between the theoretical and experimental results confirms that

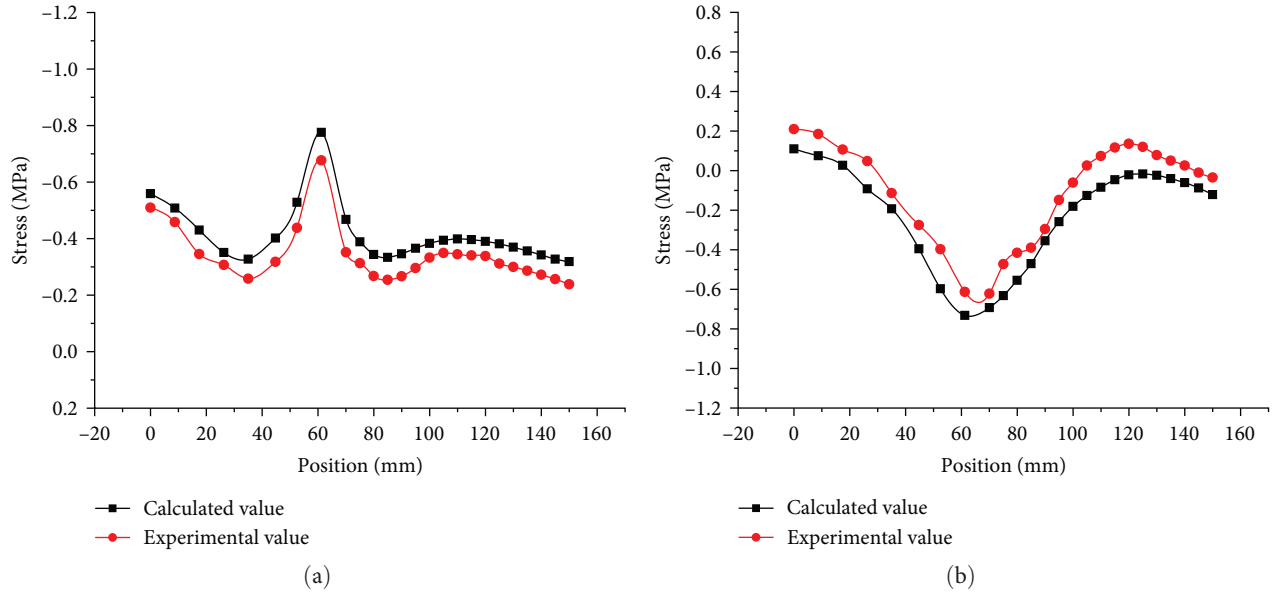

FIGURE 16: Relationship between stress and position on Section 3-3 of 4 mm model: (a) stress σ_X in X direction and (b) stress σ_Y in Y direction.

the adopted structural static analysis model is appropriate and effective.

(2) By comparing the experimental and theoretical values of the top plate displacement, it is found that under the step-by-step loading of the flat-top and four-slope folded plate structure, the displacement of the top plate has a good linear relationship with the load. As the loading force enhances, the displacement of the top plate also gradually increases. For the organic glass models with different thicknesses, under the same load, the larger the thickness, the smaller the displacement of the top plate.

(3) The mechanics characteristics of the folded plate structures with different thicknesses tend to be consistent. The maximum stress along the X and Y directions occurs at the same position, and the maximum stress value of a 3 mm thick folded plate structure is greater than that of a 4 mm thick folded plate structure. Overall, the maximum stress value of 4 mm thick folded plate structure tends to be more linear and smoother. The joint position between the top plate and slope plate of the folded plate structure is the dangerous section of structural damage, which can be reinforced with ribs to enhance its strength and prevent section failure in practical engineering.

Though some valuable insights are obtained in this work, the loosening phenomenon of the binder in the model material under the action of high load, the material performances of the plexiglass plate could not be fully exerted. Therefore, it is suggested to consider different joint treatment forms in the future model test. In the practical engineering, the folded plate structure with large thickness should be considered, and some reasonable measures can be taken to prevent structural damage for the joint position of the folded plate structure in the design and construction.

Data Availability

The data used to support the findings of this study are available from the corresponding author upon request.

Conflicts of Interest

The authors declare that they have no conflicts of interest.

Acknowledgments

The research described in this paper was financially supported by the Youth Backbone Teacher Training Program of Henan Province (2019GGJS232), Henan Province Science and Technology Research Project (232102321015, 242102321031), and Postgraduate Education Reform and Quality Improvement Project of Henan Province (YJS2023JD52, 2023SJGLX339Y).

References

[1] Y. Yang, "Introduction to folded plate structure," *Journal of Building Structure*, vol. 06, pp. 76-77, 1998.

[2] P. Bar-Yoseph and I. Hersckovitz, "Analysis of folded plate structures," *Thin-Walled Structures*, vol. 7, no. 2, pp. 139–158, 1989.

[3] C. B. Wilby, *Concrete Folded Plate Roofs*, Elsevier-Butterworth-Heinemann, Oxford, UK, 2005.

[4] P. C. Varghese, *Design of Reinforced Concrete Shells and Folded Plates*, PHI Learning Private Ltd., New Delhi, India, 2010.

[5] Y. M. Lai, Q. C. Wang, and A. L. Sun, "Internal forces and deflection of a simply-supported cross V-shaped folded plate roof," *Journal of Computational Mechanics*, vol. 04, pp. 103–109, 1997.

[6] X. Ding, T. Yu, and B. Xie, "Dynamic characteristics analysis of a new type of folded plate hollow quasi-flat reticulated shell," *China Water Transport*, vol. 23, no. 2, pp. 138-139, 2023.

[7] P. Guo, X. Ling, and Z. Y. Guo, "Prestressed concrete V folded plate composite beam roof force analysis," *Group Technology & Production Modernization*, vol. 37, no. 1, pp. 55–58, 2020.
[8] F. Miao, X. Q. Zheng, S. L. Dong, and J. Zhang, "Dynamic study on a complicated double-layer folded plate latticed shell," *Steel Construction*, vol. 31, no. 4, pp. 35–38, 2016.
[9] R. Zhu, H. G. Zhang, S. Y. Chen, L. Jiang, and Z. H. Tang, "Static characteristics and parametric analysis of folded-plated ribbed shell with inclined grid cylindrical surface," *Journal of Guangxi University*, vol. 36, no. 6, pp. 83–91, 2019.
[10] Z. J. Yu and B. Liu, "Studies on key technical problems and structural characteristics of a new folded plate latticed shell," *Structural Engineers*, vol. 28, no. 4, pp. 27–33, 2012.
[11] H. W. Zhang, W. M. Liu, H. L. Gong, W. F. Wang, and C. J. Yin, "Strain and temperature measurement and analysis of concrete structure of large-span folded plate arch tunnel side wall," *Building Technology Development*, vol. 45, no. 17, pp. 19–21, 2018.
[12] L. F. Zhang, "Dynamic performance analysis of polyhedral space folded plate structures," *Low-Carbon World*, vol. 05, pp. 147-148, 2017.
[13] I. Gaafar, "Hipped plate analysis considering joint displacement," *Transactions of the American Society of Civil Engineers*, vol. 119, no. 1, pp. 743–784, 1954.
[14] J. E. Goldberg and H. L. Leve, "Theory of prismatic folded plate structures," *International Association for Bridge and Structural Engineering*, vol. 17, pp. 59–86, 1957.
[15] A. G. Niyogi, M. K. Laha, and P. K. Sinha, "Finite element vibration analysis of laminated composite folded plate structures," *Shock and Vibration*, vol. 6, Article ID 354234, 11 pages, 1999.
[16] J. N. Bandyopadhyay and P. K. Laad, "Comparative analysis of folded plate structures," *Computers & Structures*, vol. 36, no. 2, pp. 291–296, 1990.
[17] D. D. Milašinović and S. Bursać, "Nonlinear analysis of folded-plate structures by harmonic coupled finite strip method and rheological-dynamical analogy," *Mechanics of Advanced Materials and Structures*, pp. 1–16, 2021.
[18] S. Yousif, M. P. Saka, S. Kim, and Z. W. Geem, "Optimum design of reinforced concrete folded plate structures to ACI 318-11 using soft computing algorithm," *Mathematics*, vol. 10, no. 10, Article ID 1668, 2022.
[19] Y. M. Lai, "Deflection and internal forces of simply supported truncated hip roof," *China Civil Engineering Journal*, vol. 28, no. 1, pp. 33–39, 1995.
[20] B. T. Liu and Q. F. Shi, "The experiments about roof displacement of the flat-roofed four slop-break board structure in temperature loads," *Journal of Changzhou Institute of Technology*, vol. 24, no. 2, pp. 20–23, 2011.
[21] B. T. Liu and Q. F. Shi, "The experiments about stress and strain of the flat-roofed four slop-break board structure in temperature loads," *Journal of Changzhou Institute of Technology*, vol. 25, no. 3, pp. 5–11, 2012.
[22] Y. Yang, H. Y. Li, and Y. P. Wu, "Experimental study on the mechanical behavior of truncated hip structure," *Applied Mechanics and Materials*, vol. 578-579, pp. 488–492, 2014.
[23] Y. Yang and H. Y. Li, "Study on seismic response of truncated hip structure," *Budilding Technique Development*, vol. 40, no. 12, pp. 10-11 47, 2013.
[24] A. Mesbah, Z. Belabed, K. Amara, A. Tounsi, A. Bousahla, and F. Bourada, "Formulation and evaluation a finite element model for free vibration and buckling behaviours of functionally graded porous (FGP) beams," *Structural Engineering and Mechanics*, vol. 86, no. 3, pp. 291–309, 2023.
[25] L. Q. Xia, R. Q. Wang, G. Chen, K. Asemi, and A. Tounsi, "The finite element method for dynamics of FG porous truncated conical panels reinforced with graphene platelets based on the 3-D elasticity," *Advances in Nano Research*, vol. 14, no. 4, pp. 375–389, 2023.
[26] K. Katiyar, A. Gupta, and A. Tounsi, "Microstructural/geometric imperfection sensitivity on the vibration response of geometrically discontinuous bi-directional functionally graded plates (2D-FGPs) with partial supports by using FEM," *Steel and Composite Structures*, vol. 45, no. 5, pp. 621–640, 2022.
[27] P. Van Vinh, N. Van Chinh, and A. Tounsi, "Static bending and buckling analysis of bi-directional functionally graded porous plates using an improved first-order shear deformation theory and FEM," *European Journal of Mechanics—A/Solids*, vol. 96, Article ID 104743, 2022.